Magnetic properties and electronic structures of intermediate valence systems $CeRhSi_2$ and $Ce_2Rh_3Si_5$

2010 J. Phys.: Condens. Matter 22 215601

(http://iopscience.iop.org/0953-8984/22/21/215601)

J. Phys.: Condens. Matter **22** (2010) 215601 (11pp) doi:10.1088/0953-8984/22/21/215601

Magnetic properties and electronic structures of intermediate valence systems $CeRhSi_2$ and $Ce_2Rh_3Si_5$

D Kaczorowski[1], A P Pikul[1], U Burkhardt[2], M Schmidt[2], A Ślebarski[3], A Szajek[4], M Werwiński[4] and Yu Grin[2]

[1] Institute of Low Temperature and Structure Research, Polish Academy of Sciences, PO Box 1410, 50-950 Wrocław, Poland
[2] Max Planck Institute for Chemical Physics of Solids, Nöthnitzer Straße 40, D-01187 Dresden, Germany
[3] Institute of Physics, University of Silesia, 40-007 Katowice, Poland
[4] Institute of Molecular Physics, Polish Academy of Sciences, M. Smoluchowskiego 17, 60-179 Poznań, Poland

E-mail: D.Kaczorowski@int.pan.wroc.pl

Received 8 March 2010
Published 5 May 2010
Online at stacks.iop.org/JPhysCM/22/215601

Abstract
The crystal structures and the physical (magnetic, electrical transport and thermodynamic) properties of the ternary compounds $CeRhSi_2$ and $Ce_2Rh_3Si_5$ (orthorhombic $CeNiSi_2$- and $U_2Co_3Si_5$-type structures, respectively) were studied over wide ranges of temperature and magnetic field strength. The results revealed that both materials are valence fluctuating systems, in line with previous literature reports. Direct evidence for valence fluctuations was obtained by means of Ce L_{III}-edge x-ray absorption spectroscopy and Ce 3d core-level x-ray photoelectron spectroscopy. The experimental data were confronted with the results of *ab initio* calculations of the electronic band structures in both compounds.

(Some figures in this article are in colour only in the electronic version)

1. Introduction

The system Ce–Rh–Si is known to be exceptionally rich in ternary phases, which scan a full spectrum of magnetic behavior related to the hybridization of cerium 4f electronic states with d and p states of neighboring atoms. The most intensively studied so far has been the tetragonal compound $CeRh_2Si_2$, which is considered as an archetypal example of pressure-induced superconductivity emerging from a magnetically ordered state [1]. At ambient pressure, the 4f electrons in $CeRh_2Si_2$ are well localized and give rise to an antiferromagnetic ordering setting in at $T_{N1} = 36$ K that is followed by a change of the magnetic structure at $T_{N2} = 25$ K [2]. Under high pressure one observes a gradual suppression of the Néel temperature down to absolute zero in the vicinity of the critical pressure $p_c \approx 1$ GPa [3]. Most interestingly, in the quantum critical region near p_c the compound becomes superconducting below $T_c = 0.5$ K [3, 4]. Simultaneously, the Fermi surface topology varies abruptly and the cyclotron mass measured in the de Haas–van Alphen experiment increases rapidly, hence manifesting a change in character of the 4f electrons, which become itinerant in the critical region [5]. Another pressure-induced superconductor among the Ce–Rh–Si ternaries is $CeRhSi_3$ [1]. At ambient pressure, this tetragonal compound orders antiferromagnetically at $T_N = 1.6$ K and behaves as a Kondo lattice with a characteristic temperature T_K of about 100 K [6]. In contrast to the case of $CeRh_2Si_2$, at an applied pressure T_N does not change monotonically: it first increases up to 1.9 K near 0.8 GPa and then decreases down to 1.1 K near 2.6 GPa without further change at higher pressures [8]. Most importantly, superconductivity appears in this compound already under small pressures and coexists with the antiferromagnetic ordering in the entire pressure range studied, with the critical temperature gradually rising up to 1.1 K with increasing pressure [8]. Above

2.6 GPa, T_c merges with T_N [7, 8]. Moreover, in the vicinity of this pressure, pronounced non-Fermi liquid features are observed in all the bulk properties. The occurrence of superconductivity in $CeRhSi_3$ is highly peculiar, as the crystal structure of this compound lacks an inversion symmetry [8]. Apparently, $CeRhSi_3$ is another member of a novel family of unconventional non-centrosymmetric superconductors, with the most prominent representative being $CePt_3Si$ [9]. Likely, mixed spin-triplet pairing symmetry in $CeRhSi_3$ is responsible for the extremely large upper critical magnetic field $B_{c2}(0) = 30$ T measured in a magnetic field applied along the crystallographic c axis, its very unusual temperature dependence, as well as the strong anisotropy of $B_{c2}(0)$ (cf $B_{c2}(0) = 7$ T for $B \perp c$-axis) [10].

Motivated by the intriguing physics in $CeRh_2Si_2$ and $CeRhSi_3$, we started systematic investigations of the physical behavior in other ternaries from the Ce–Rh–Si phase diagram. Recently, we reported on very complex magnetic properties of the orthorhombic compound $CeRh_3Si_2$, marked by two subsequent antiferromagnetic phase transitions at $T_{N1} = 4.7$ K and $T_{N2} = 4.5$ K, multiple metamagnetic transitions in the ordered state and a huge magnetocrystalline anisotropy being quite uncommon for Ce-based intermetallics [11]. In turn, for hexagonal Ce_2RhSi_3 we provided evidence of Kondo lattice behavior with the characteristic temperature $T_K \approx 9$ K, which coexists below $T_N = 4.5$ K with long-range antiferromagnetic ordering [12]. Remarkably, by means of bulk and spectroscopic measurements, the cerium 4f electrons were found to be well localized in both compounds.

An entirely opposite character of the 4f states may be expected for the silicides $CeRhSi_2$ and $Ce_2Rh_3Si_5$, which have been reported in the literature as valence fluctuating systems [13–16]. The former compound crystallizes with an orthorhombic crystal structure of the $CeNiSi_2$ type. Its unit cell volume does not follow the lanthanide contraction established for the $RERhSi_2$ (RE = La, Pr, Nd) series. The magnetic susceptibility of $CeRhSi_2$ shows a non-Curie–Weiss temperature variation with a broad maximum near 80 K. The electrical resistivity is proportional to the squared temperature below about 50 K, while above 100 K it decreases slightly with increasing temperature. These features of the bulk magnetic and electrical behaviors reflect the instability of the Ce ions' valence. The Coqblin–Schrieffer approach applied to the magnetic data of $CeRhSi_2$ yielded the characteristic temperature $T_0 = 309$ K (T_0 is related to the Kondo temperature T_K via the Wilson number, $T_K = WT_0$). In turn, analysis of the resistivity data in terms of the Freimuth model gave estimates for the spin fluctuation temperature $T_{sf} = 147$ K and the position of the 4f band with respect to the Fermi energy $T_f = 30$ K. The valence fluctuating nature of $CeRhSi_2$ has also been concluded in an independent study reported in [14]. The other compound of interest, i.e. $Ce_2Rh_3Si_5$, was studied in less detail. It was reported to form with the orthorhombic $U_2Co_3Si_5$-type structure as a member of the $RE_2Rh_3Si_5$ (RE = La–Er) family. As the lattice parameters of its unit cell follow the lanthanide contraction along the series it was concluded in [15] that the Ce ions in this compound are trivalent. On the other hand, the same authors reported nearly temperature-independent magnetic susceptibility of $Ce_2Rh_3Si_5$, and in order to reconcile their contradictory findings they speculated that the ground state in this compound is nonmagnetic because of the presence of 'virtual' spin fluctuations, which, however, do not destabilize the charge state of the Ce ions. The electrical transport properties of $Ce_2Rh_3Si_5$ were reported in [16]. In the temperature range 2–30 K, the resistivity was shown to vary as T^3 and were interpreted as being governed by interband s–d scattering. The nonmagnetic character of $Ce_2Rh_3Si_5$ was also inferred from the heat capacity data, which show featureless temperature behavior up to 30 K and strongly reduced entropy $S(30\text{ K}) = 0.24R$.

In this work we reinvestigated the magnetic and electrical transport properties of $CeRhSi_2$ and $Ce_2Rh_3Si_5$. Moreover, we measured for the first time the specific heat of both materials in a wide temperature range 0.35–300 K, and performed x-ray absorption spectroscopy (XAS) and x-ray photoelectron spectroscopy (XPS) studies. The experimental data are discussed in the context of the calculated electronic structures. Altogether, the obtained results confirm the valence fluctuating nature of both compounds.

2. Experimental and computational details

Polycrystalline samples of $CeRhSi_2$ and $Ce_2Rh_3Si_5$ were prepared by arc melting stoichiometric amounts of the elemental components (Ce—3N, Ames Laboratory, Rh—3N, Chempur and Si—6N, Chempur) in a copper-hearth furnace installed inside a glove-box filled with ultra-pure argon gas with continuously controlled partial pressures of O_2 and H_2O to be lower than 1 ppm. The buttons were flipped over and remelted several times to ensure good homogeneity. The weight losses after the final melting were negligible (less than 0.2%).

The quality of the obtained alloys was checked by x-ray powder diffraction on an X'pert Pro PANalytical diffractometer with Cu Kα radiation and by energy dispersive x-ray (EDX) analysis using a Philips 515 scanning electron microscope equipped with an EDAX PV 9800 spectrometer. Both techniques proved the single-phase character of the $Ce_2Rh_3Si_5$ sample, with the expected stoichiometry and crystal structure. In the case of $CeRhSi_2$, however, some small admixture of $CeRh_2Si_2$ was found in the x-ray pattern and the EDX spectrum. The structural refinements were done by employing the program FULLPROF [17].

Magnetic susceptibility measurements were performed in the temperature range 1.72–800 K in magnetic fields of 0.5 T using a Quantum Design superconducting quantum interference device (SQUID) magnetometer. The heat capacity and the electrical resistivity were measured within the temperature interval 2–300 K using a Quantum Design PPMS platform.

The x-ray photoelectron spectroscopy experiments were carried out at room temperature using a Physical Electronics PHI 5700/660 spectrometer with monochromatized Al Kα radiation (1486.6 eV). The spectra were collected on parallelepiped-shaped specimens broken *in situ* in a high vacuum of the order of 10^{10} Torr.

Table 1. Atomic positions and equivalent isotropic thermal displacement parameters for $CeRhSi_2$.

Atom	Site	x	y	z	U(eq)
Ce	4c	0	0.8945(1)	0.75	0.0108(6)
Rh	4c	0.5	0.8211(1)	0.25	0.037(1)
Si1	4c	0	0.5427(7)	0.75	0.032(4)
Si2	4c	0.5	0.7477(5)	0.75	0.010(3)

The measurements of the x-ray absorption spectroscopy at the Ce-L_{III} threshold were performed at several different temperatures at the EXAFS-1 beamline C of the Hamburger Synchrotronstrahlungslabor (HASYLAB/DESY) using a fixed-exit double-crystal Si(111) monochromator. In these studies CeO_2 and CeF_3 were used as the internal standards. The energy scans were made step-by-step with an energy resolution of approx. 1 eV. The absorption spectra were calculated by $\ln(C_1/C_2)$ from the x-ray intensities C_1, C_2, detected by ionization chambers in front and behind the irradiated flat sample. A peak-to-background ratio $P/B = 0.6$ at the Ce-L_{III} white line was realized with powdered samples of about 16 mg, which were mixed with small amounts of B_4C and fixed with paraffin wax on a 1 cm^2 window of the flat copper sample holder. Temperatures in the range 5–293 K were obtained by an He-gas flow cryostat showing a thermal stability of $T = \pm 0.5$ K during typical measuring dwell times of 20 min.

The electronic structure calculations were performed within density functional theory [18] using the full-potential local-orbital minimum-basis band structure scheme (FPLO) [19] and the full-potential linearized augmented plane wave (LAPW) method implemented in the latest version (WIEN2k) of the original WIEN code [20]. The FPLO calculations were performed in the fully relativistic mode and the LSDA (the local spin density approximation) exchange–correlation potential was assumed in the form proposed by Perdew and Wang [21]. In the WIEN2k code calculations the scalar relativistic approach was implemented with the spin–orbit interactions taken into account using the second variational method [22]. Two different exchange–correlation potentials in the generalized gradient approximation (GGA) were tested, in the forms proposed by Perdew *et al* [23] as well as Wu and Cohen [24]. Furthermore, to improve the description of the strongly correlated 4f electrons, the on-site Coulomb energy U correction was introduced within the LSDA + U approach [25]. The value of U_{eff} was chosen equal to 6 eV [26]. The number of k-points was 8000 in the Brillouin zone (BZ), which corresponds to at least 1100 points in the irreducible wedge of the BZ for all systems and methods of calculations. For BZ integration a tetrahedron method was used [27]. The self-consistent criterion was equal to at least 10^{-6} Ryd for the total energy. The calculations were performed for lattice constants and atomic positions in the unit cells as given in section 3.1.

The theoretical photoemission spectra (XPS) were obtained from the calculated densities of electronic states (DOS) convoluted by Gaussians with a half-width (δ) equal to 0.3 eV and scaled using the proper photoelectronic cross sections for partial states [28].

Table 2. Atomic positions and equivalent isotropic thermal displacement parameters for $Ce_2Rh_3Si_5$.

Atom	Site	x	y	z	U(eq)
Ce	8j	0.2668(1)	0.1305(1)	0	0.0072(3)
Rh1	4a	0	0	0.75	0.0097(6)
Rh2	8j	0.3923(1)	0.1386(2)	0.5	0.0108(4)
Si1	4b	0.5	0	0.75	0.018(2)
Si2	8g	0	0.2218(4)	0.75	0.017(2)
Si3	8j	0.1574(6)	0.1095(6)	0.5	0.021(2)

3. Results and discussion

3.1. Crystal structures

The compound $CeRhSi_2$ was reported in the literature to crystallize with an orthorhombic structure of $CeNiSi_2$ type [13, 14]. In turn, $Ce_2Rh_3Si_5$ was considered as having an orthorhombic structure isotypic to $U_2Co_3Si_5$ [15, 16]. However, to the best of our knowledge, for none of these two phases were any details on the atomic positions in the unit cells reported. Therefore, the x-ray powder diffraction data obtained in the present study as part of the characterization of the samples' quality were used to refine the crystal structures of both compounds.

For $CeRhSi_2$, the refined lattice parameters are $a = 4.2615(3)$ Å, $b = 16.7469(9)$ Å and $c = 4.1751(3)$ Å, in good agreement with those given in [14]. The crystal structure belonging to the space group $Cmcm$ was refined down to the residuals $R_{\mathrm{p}} = 3.4\%$ and $R_{\mathrm{wp}} = 5.3\%$. The obtained atomic coordinates are given in table 1, together with the values of equivalent isotropic thermal displacement parameters for all the atoms. The compound was thus confirmed to be isostructural with $CeNiSi_2$. Detailed discussion of this crystal structure can be found in the literature, e.g. in the original paper [29]. For the purpose of this work it is enough to note that the unit cell contains one position of Ce atoms, which are coordinated by four Rh atoms at a distance of 3.226 Å, four Si1 atoms at a distance of 3.163 Å and two Si2 atoms at a distance of 3.167 Å.

As for $Ce_2Rh_3Si_5$, the unit cell of the $U_2Co_3Si_5$ type (space group $Ibam$) has also been corroborated. The crystal structure was refined down to the residuals $R_{\mathrm{p}} = 2.3\%$ and $R_{\mathrm{wp}} = 3.1\%$. The obtained lattice parameters are $a = 9.8949(3)$ Å, $b = 11.7576(3)$ Å and $c = 5.8114(1)$ Å. These values differ only slightly from those reported in [15, 16]. The atomic coordinates and the equivalent isotropic thermal displacement parameters are collected in table 2. In the unit cell of $Ce_2Rh_3Si_5$ there is one position of the Ce atom that is surrounded by one Rh2 atom at a distance of 3.138 Å, two Rh2 atoms at a distance of 3.161 Å, one Rh2 atom at a distance of 3.375 Å, two Rh1 atoms at a distance of 3.381 Å and one Rh2 atom at a distance of 3.399 Å. The nearest-neighbor silicon atoms are located at the distances: 3.022 Å (one Si3 atom), 3.111 Å (two Si3 atoms), 3.129 Å (one Si1 atom), 3.148 Å (one Si3 atom), 3.199 Å (two Si2 atoms) and 3.233 Å (one Si2 atom). Further details on the $U_2Co_3Si_5$-type crystal structure can be found in the literature (see, e.g., [16]).

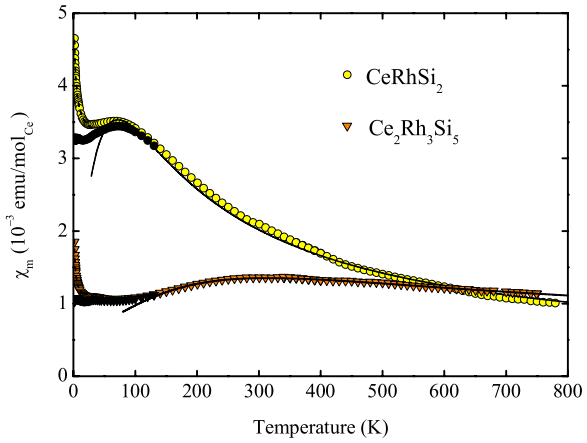

Figure 1. Temperature dependences of the molar magnetic susceptibility of $CeRhSi_2$ and $Ce_2Rh_3Si_5$. The full symbols represent the $\chi(T)$ curves corrected for contributions coming from spurious Ce^{3+} ions (see text for details). The dashed and solid lines are the fits discussed in the text.

3.2. Magnetic properties

The magnetic data of $CeRhSi_2$ and $Ce_2Rh_3Si_5$ are summarized in figure 1. The compounds exhibit small (of the order of 10^{-3} emu mol^{-1} per Ce atom) and weakly temperature-dependent magnetic susceptibility that clearly manifests the nonmagnetic character of both materials. With decreasing temperature from 800 K the susceptibility of $CeRhSi_2$ slightly increases, goes through a broad maximum centered around 75 K and then rapidly rises below about 20 K. Similar behavior is observed for $Ce_2Rh_3Si_5$, with a maximum located around 270 K and some tendency for saturation before the low-temperature upturn occurs. The overall shape of these $\chi(T)$ curves is typical for Ce-based intermetallics with valence fluctuations. The position of the maximum in $\chi(T)$, $T(\chi^{\max})$, gives an estimate for the characteristic temperature $T_{\rm sf}$, related to spin fluctuations in such compounds. From the relation [30]

$$T_{\rm sf} = \tfrac{3}{2} T(\chi^{\max}) \tag{1}$$

one finds $T_{\rm sf} \simeq 112$ K for $CeRhSi_2$ and $T_{\rm sf} \simeq 405$ K for $Ce_2Rh_3Si_5$. Comparison of these values suggests that in these two compounds interactions of the cerium 4f electrons with the conduction band is stronger in the latter one, in line with the smaller and less temperature-dependent magnetic susceptibility observed for $Ce_2Rh_3Si_5$.

Low-temperature upturns in $\chi(T)$ curves are commonly observed in Ce-based intermediate valence materials and their origin is usually attributed to the presence of stable Ce^{3+} ions located at grain boundaries and/or some contamination by paramagnetic impurities. To account for this spurious effect it is assumed that the intrinsic susceptibility of $CeRhSi_2$ and $Ce_2Rh_3Si_5$ at low temperatures is given by the formula [31]

$$\chi(0) = \frac{C}{2T_{\rm sf}} \tag{2}$$

in which $C = 0.807$ emu mol^{-1} K^{-1} stands for the Curie constant of free Ce^{3+} ions ($C = \frac{N\mu_{\rm eff}^2}{3k_{\rm B}}$, where N is the Avogadro number and $k_{\rm B}$ is the Boltzmann constant, while $\mu_{\rm eff} = 2.54\ \mu_{\rm B}$ is the effective magnetic moment of the cerium $4f^1$ state). The above-derived values of $T_{\rm sf}$ imply $\chi(0)$ equal to 3.6×10^{-3} emu mol^{-1} for $CeRhSi_2$ and 1.0×10^{-3} emu mol^{-1} per Ce atom for $Ce_2Rh_3Si_5$. Then, the measured magnetic susceptibility can be modeled by the function

$$\chi(T \to 0) = \chi(0) + \frac{nC}{T}, \tag{3}$$

where the Curie term represents the contribution due to spurious Ce^{3+} ions in an amount of n atoms per mole of the given compound. Fitting this equation to the experimental data taken below 20 K (note the dashed lines in figure 1) yields $n = 6.3 \times 10^{-3}$ and 3.5×10^{-3} for $CeRhSi_2$ and $Ce_2Rh_3Si_5$, respectively. The magnetic susceptibility data corrected for the spurious Ce^{3+} ions is shown in figure 1 by the full symbols.

At higher temperatures the magnetic susceptibility of both compounds can be analyzed in terms of the interconfiguration fluctuations (ICF) model developed for intermediate valence systems by Sales and Wohlleben [32]. Within this approach the magnetic susceptibility of a Ce-based compound with nonmagnetic $4f^0$ ground state is expressed as

$$\chi(T) = \frac{C[1 - \nu(T)]}{T + T_0} + \chi_0, \tag{4}$$

where T_0 is a characteristic temperature associated with valence fluctuations between the $4f^0$ and $4f^1$ configurations of Ce ions, whereas $\nu(T)$ stands for the temperature-dependent mean occupation of the ground state that is given by the formula

$$\nu(T) = \frac{1}{1 + 6\exp(\frac{-E_{\rm ex}}{T+T_0})} \tag{5}$$

in which $E_{\rm ex}$ denotes the energy difference between the ground and excited states. The constant term χ_0 in equations (4) accounts for the paramagnetic contribution due to conduction electrons and the diamagnetic contribution due to core electrons. Fitting the ICF model to the experimental data of $CeRhSi_2$ and $Ce_2Rh_3Si_5$ resulted in reasonable descriptions of the magnetic behavior above about 50 K and 150 K, respectively (note the solid lines in figure 1). The parameters obtained in the least-squares fits are $E_{\rm ex} = 220$ K, $T_0 = 44$ K and $\chi_0 = 2.3 \times 10^{-4}$ emu mol^{-1} for the former compound, and $E_{\rm ex} = 845$ K, $T_0 = 129$ K and $\chi_0 = 4.9 \times 10^{-4}$ emu mol^{-1} for the latter one. Assuming that the highest possible valence for the cerium $4f^0$ state is +3.30 (for a discussion see [33]), one may estimate from equation (5) the change of the effective valence of Ce ions with varying temperature. In the range in which the ICF model provides a proper approximation of the susceptibility of the compounds studied one finds for $CeRhSi_2$ the valence change from +3.19 at 50 K to +3.07 at 300 K and to +3.05 at 800 K, while for $Ce_2Rh_3Si_5$ the change is from +3.23 at 150 K to +3.16 at 300 K and to +3.09 at 800 K.

3.3. Heat capacity

Figure 2 displays the temperature dependences of the specific heat of $CeRhSi_2$ and $Ce_2Rh_3Si_5$. The solid lines through the experimental points are the least-squares fits of the formula

$$C(T) = C_{\rm el}(T) + C_{\rm ph}(T), \tag{6}$$

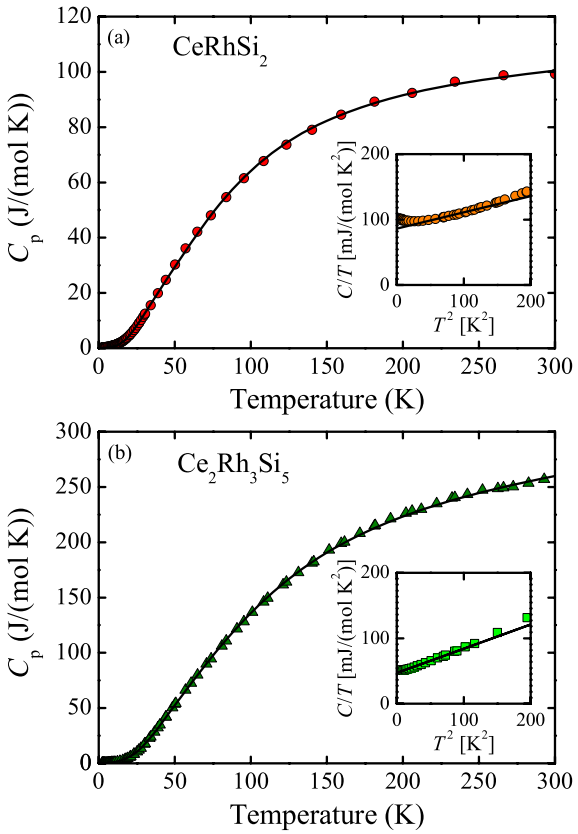

Figure 2. Temperature dependences of the specific heat of (a) $CeRhSi_2$ and (b) $Ce_2Rh_3Si_5$. The insets present the low-temperature data in the form C/T versus T^2. The solid lines are the fits discussed in the text.

where the first term is the electron specific heat $C_{\rm el}(T) = \gamma T$, while the second one represents the phonon contribution in the form [34, 35]

$$C_{\rm ph}(T) = \frac{1}{1-\alpha T}\Bigg[\underbrace{9R\left(\frac{T}{\Theta_{\rm D}}\right)^3\int_0^{\Theta_{\rm D}/T}\frac{x^4{\rm e}^x}{({\rm e}^x-1)^2}\,{\rm d}x}_{C_{\rm ph,D}} + \underbrace{\sum_i n_{{\rm E}i}R\left(\frac{\Theta_{{\rm E}i}}{T}\right)^2\frac{{\rm e}^{\Theta_{{\rm E}i}/T}}{({\rm e}^{\Theta_{{\rm E}i}/T}-1)^2}}_{C_{\rm ph,E}}\Bigg]. \quad (7)$$

Here, α stands for the anharmonic coefficient, R is the gas constant, $C_{\rm ph,D}$ describes the Debye contribution of three acoustic modes (characterized by the Debye temperature $\Theta_{\rm D}$) and $C_{\rm ph,E}$ represents the Einstein specific heat calculated for i groups with n_i optical branches (characterized by the Einstein temperatures $\Theta_{{\rm E}i}$). In order to avoid overparameterization of the experimental curves $C(T)$ (figure 2), we reduced the number of groups of optical branches to $i = 2$, which seems to be the minimum to describe satisfactorily the specific heat data. In that case we found that the best results one obtains assuming multiplicity $n_1 = 2$ and $n_2 = 7$ in $CeRhSi_2$, and $n_1 = 12$ and $n_2 = 15$ in $Ce_2Rh_3Si_5$. The so-obtained explicit form of equation (6) applied to the experimental data above about 15 K yields for $CeRhSi_2$ the fitting parameters: $\Theta_{\rm D} = 163$ K, $\Theta_{{\rm E}_1} = 139$ K, $\Theta_{{\rm E}_2} = 324$ K, $\gamma = 22.4$ mJ mol^{-1} K^{-2} and $\alpha \approx 1.0 \times 10^{-6}$ K^{-1}. In the case of $Ce_2Rh_3Si_5$ a reasonable fit to the experimental data was obtained with $\Theta_{\rm D} = 147$ K, $\Theta_{{\rm E}_1} = 198$ K, $\Theta_{{\rm E}_2} = 427$ K, $\gamma = 45.3$ mJ mol^{-1} K^{-2} and $\alpha = 2.7 \times 10^{-4}$ K^{-1}. It is worthwhile emphasizing that the presented model does not reflect the complexity of the real lattice vibrations in the two compounds, and at most gives only basic characteristics of the phonon spectra.

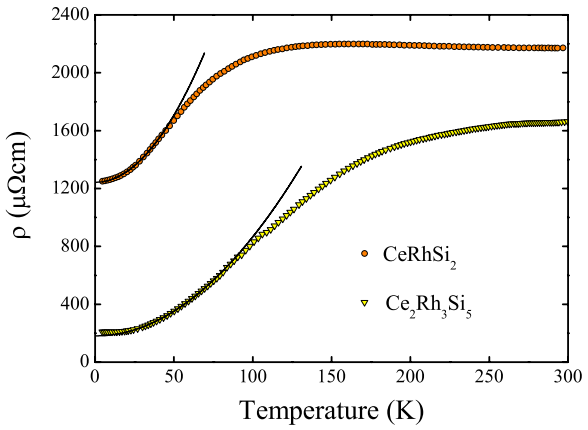

Figure 3. Temperature dependences of the electrical resistivity of $CeRhSi_2$ and $Ce_2Rh_3Si_5$. The solid lines are the fits discussed in the text.

As can be inferred from the insets to figure 2, below about 12 K the experimental specific heat data can be described by a simple formula

$$C(T)/T = \gamma + r\frac{1944}{\Theta_{\rm D,LT}^3}T^2, \quad (8)$$

where the second term is the conventional T^3-Debye law with the low-T Debye temperature $\Theta_{\rm D,LT}$ and r stands for a number of atoms in a formula unit [34, 35]. The insets to figure 2 present the least-squares fits of the latter formula to the measured specific heat data with the parameters $\gamma = 86$ mJ mol^{-1} K^{-2} and $\Theta_{\rm D,LT} = 315$ K for $CeRhSi_2$ and $\gamma = 47$ mJ mol^{-1} K^{-2} and $\Theta_{\rm D,LT} = 375$ K for $Ce_2Rh_3Si_5$. The obtained values of $\Theta_{\rm D,LT}$ are obviously different from those obtained using previous full-range fittings since in the latter approximation only the acoustic branches are considered, and thus $\Theta_{\rm D,LT}$ reflects an average characteristic temperature of the phonon spectrum. The obtained γ coefficients are in both compounds of the order typical for systems with valence fluctuations [36, 37].

At low temperatures approaching the experimental limit a little upturn is observed in $C(T)/T$ of $CeRhSi_2$. This anomaly has an unknown origin and can temporarily be ascribed to the impurity phase $CeRh_2Si_2$, detected in the x-ray diffraction pattern of the sample measured. However, an intrinsic nature of the upturn can neither be excluded.

3.4. Electrical resistivity

The temperature variations of the electrical resistivity of $CeRhSi_2$ and $Ce_2Rh_3Si_5$ are shown in figure 3. For both compounds the absolute magnitude of the resistivity is very

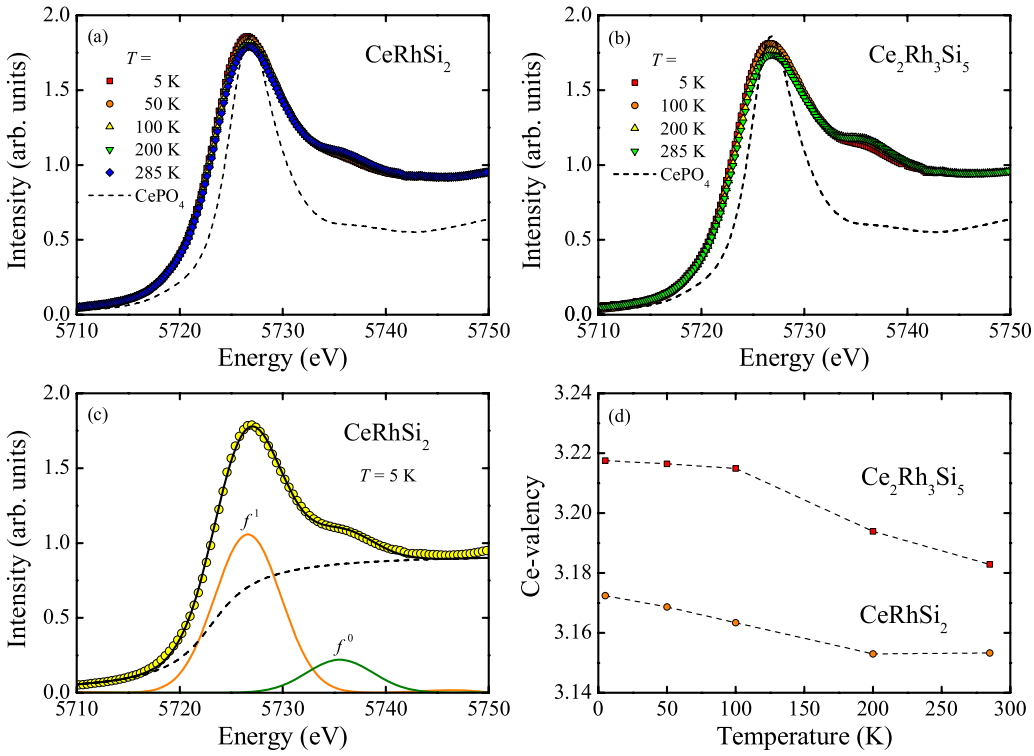

Figure 4. X-ray absorption spectra at the Ce-L_{III} threshold measured at various temperatures for (a) $CeRhSi_2$ and (b) $Ce_2Rh_3Si_5$. The standard spectrum for Ce^{3+} ions, i.e. that of $CePO_4$, is represented by the dashed curves. As an example, deconvolution of the spectrum measured for $CeRhSi_2$ at 5 K is shown in panel (c). The contributions due to 4 f^1 and 4 f^0 configurations are depicted by the solid lines, while the dashed line represents the arctan function accounting for transitions of the 2p electrons to the conduction band. Panel (d) displays the calculated changes of the Ce ions' valence in both compounds with varying temperature.

high because of many cracks present in the specimens measured (the samples were very brittle). Therefore, quantitative discussion of the electrical behavior of these silicides is not possible. Nevertheless, it is clear that both materials exhibit metallic-like conductivity with some features characteristic of valence fluctuations systems [36, 37]. Below 50 K for $CeRhSi_2$ and 90 K for $Ce_2Rh_3Si_5$ K the resistivity is proportional to the squared temperature, as predicted for such systems within the paramagnon model [30] (some deviations from $\rho \sim T^2$ are observed below 10 K and 20 K, respectively). At higher temperatures the $\rho(T)$ curve of $CeRhSi_2$ forms a broad shallow maximum above 100 K, while that of $Ce_2Rh_3Si_5$ shows a tendency to saturate near room temperature. The observed behavior is thus fully consistent with the values of the spin fluctuation temperature $T_{sf} \simeq 112$ K and $T_{sf} \simeq 405$ K estimated from the magnetic susceptibility data for the former and the latter compound, respectively.

3.5. XAS spectra

The x-ray absorption spectroscopy data obtained for $CeRhSi_2$ and $Ce_2Rh_3Si_5$ are gathered in figure 4. For each compound a linear baseline determined at 100 eV below the Ce-L_{III} absorption edge was subtracted and the spectrum was normalized to the intensity values at $E = 5755$ eV. The absorption spectra of both phases show one dominant white line at 5726 eV of the Ce-L_{III} line and several maxima with energies higher than 5750 eV in the extended x-ray absorption fine structure (EXAFS) region. The EXAFS signal is influenced by specific features of the crystal structure of the investigated compound. Comparison of the measured spectrum with that of the Ce^{3+} reference system $CePO_4$ allows us to attribute the observed white line to the same dominant $4f^1$ electronic configuration of the cerium atoms. Both phases, i.e. $CeRhSi_2$ and $Ce_2Rh_3Si_5$, thus show a mean valence of cerium ions relatively close to +3. However, the presence of an additional contribution at nearly $\Delta E \approx 9$ eV above the white line maximum clearly shows mixed valent behavior of the compounds investigated. Decreasing the temperature from room temperature to $T = 5$ K leads to a small decrease in the intensity of the white line and a simultaneous increase of the other peak. The observed shift of the spectral weight of the Ce-L_{III} white line to higher energies implies a reduced influence of the 4f electron on the 2p $\rightarrow$ *n*d transition. This behavior manifests a gradual gain in the contribution due to the $4f^0$ configuration, and thus reflects an increase of the mean valence of the Ce atoms with decreasing temperature.

In quantitative evaluation of the spectra measured for $CeRhSi_2$ and $Ce_2Rh_3Si_5$, two Gaussian functions were considered, which represent the $4f^1$ and $4f^0$ contributions, respectively (see an example presented in panel (c) of figure 4). Additionally, an arctan function was added in order to account for the contribution due to transitions of the 2p electrons to the conduction band. Analyzing the relative increase of the $4f^0$ peak with decreasing temperature one obtains for $CeRhSi_2$ the mean valence of Ce ions changing from +3.15

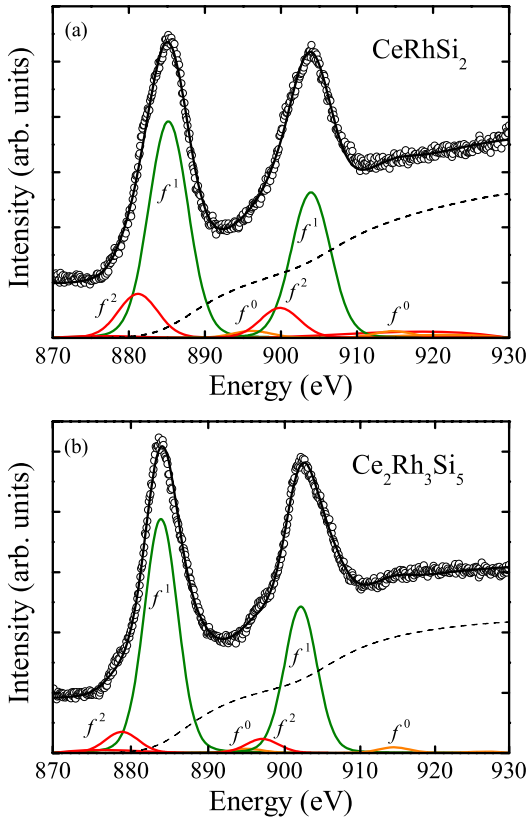

Figure 5. Ce 3d XPS spectra obtained for (a) $CeRhSi_2$ and (b) $Ce_2Rh_3Si_5$. The f^0, f^1 and f^2 components were separated on the basis of Doniach–Šunjić theory.

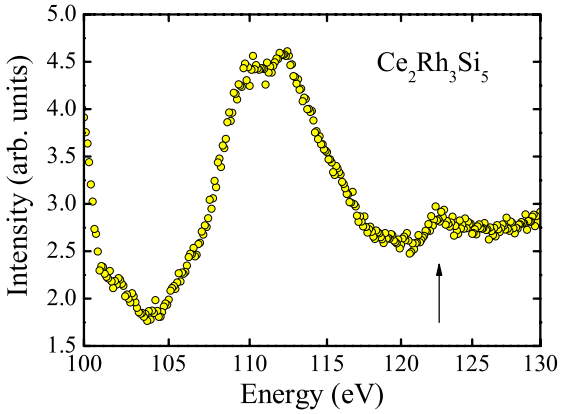

Figure 6. Ce 4d XPS spectrum obtained for $Ce_2Rh_3Si_5$.

at room temperature to +3.17 at 5 K (see figure 4(d)). A similar calculation performed for $Ce_2Rh_3Si_5$ yields the valence increase from +3.18 at 280 K to +3.22 at 5 K (cf figure 4(b)).

3.6. XPS spectra

The XPS spectra of the 3d core levels usually provide some detailed information about the 4f shell configurations and the f-conduction-electron hybridization. The calculations by Gunnarsson and Schönhammer [38] indicate that a large hybridization potential, V_{fs}, is necessary to explain the observed spectra for several Ce-intermetallic compounds, which often show different final states depending on the occupation of the f shell: f^0, f^1 and f^2 (see [39]). Due to the spin–orbit (SO) interaction there are two sets of Ce 3d photoemission lines in the spectrum attributed to the $3d_{3/2}$ and $3d_{5/2}$ components of the final states, with an intensity ratio $I(3d_{5/2})/I(3d_{3/2}) = 3/2$. The main photoemission lines originating from Ce^{3+} are labeled as $3d4f^1$.

The $3d4f^2$ final state components appears when the core hole becomes screened by an additional 4f electron, which is possible due to the hybridization of the Ce 4f shell with the conduction electrons. Consequently, the $3d^9f^2$ components in the Ce 3d XPS spectra are attributed within the Gunnarsson–Schönhammer model to the f-conduction-electron hybridization energy Δ_{fs}. $\Delta_{fs} = \pi V^2 \rho_{max}$ describes the hybridization part of the Anderson impurity Hamiltonian [40], where ρ_{max} is the maximum in the DOS and V is the hybridization matrix element. It is possible to estimate Δ_{fs} from the ratio $r = I(f^2)/(I(f^1) + I(f^2))$, calculated as a function of Δ_{fs} in [39], when the peaks of the Ce 3d XPS spectra that overlap are separated.

Figure 5 shows the Ce 3d XPS spectra of $CeRhSi_2$ (a) and $Ce_2Rh_3Si_5$ (b). The separation of the overlapping peaks in the spectra was done on the basis of Doniach–Šunjić theory [41]. A background, calculated using the Tougaard algorithm [42], was subtracted from the XPS data. The estimated value of the SO splitting equals 18.6 eV. In figure 5 each SO set of the Ce 3d photoemission lines consists of contributions marked as f^0, f^1 and f^2. The intensity ratio $r \approx 0.09$ for $CeRhSi_2$ and ∼0.17 for $Ce_2Rh_3Si_5$. This intensity ratio gives for $CeRhSi_2$ and $Ce_2Rh_3Si_5$ a crude estimate of a hybridization width $\Delta_{fs} \sim$ 40 meV and ∼83 meV, respectively. The estimated energy Δ_{fs} for $Ce_2Rh_3Si_5$ is twice as large as the value for $CeRhSi_2$, which suggests a lower occupation number n_f of the 4f shell in $Ce_2Rh_3Si_5$.

In order to determine the ground state f occupation from the 3d XPS spectra we use figures 4 and 6 of [39], where the dependence of the ratio $I(f^0)/[I(f^0) + I(f^1) + I(f^2)]$ on the f occupation is shown for different Δ_{fs}. Relative f^0 intensities of magnitude ∼0.05 for $CeRhSi_2$ and ∼0.07 for $Ce_2Rh_3Si_5$ correspond to n_f values of the order of 0.95 and 0.93, respectively. The Ce 3d XPS spectra, however, allow an estimate of the occupation number n_f (and of the energy Δ_{fs}) within an accuracy of the order of 20%. The errors due to the uncertainties in the intensity ratios we discussed previously [43].

We note, however, that the n_f value obtained from the Ce 3d XPS spectra is smaller than that estimated from the x-ray absorption spectra either for $CeRhSi_2$ or $Ce_2Rh_3Si_5$. This discrepancy shows immediately that the final state f occupation is a different function of the initial state occupancy for each type of spectroscopy (see [44]). We note, however, that the n_f value for $CeRhSi_2$ is larger than n_f derived for $Ce_2Rh_3Si_5$.

Other evidence for a fluctuating valence in $Ce_2Rh_3Si_5$ comes from the Ce 4d XPS data. As shown in figure 6, the latter spectrum exhibits some features above 120 eV (marked by the arrow), which can be assigned to the f^0 final state [45, 46].

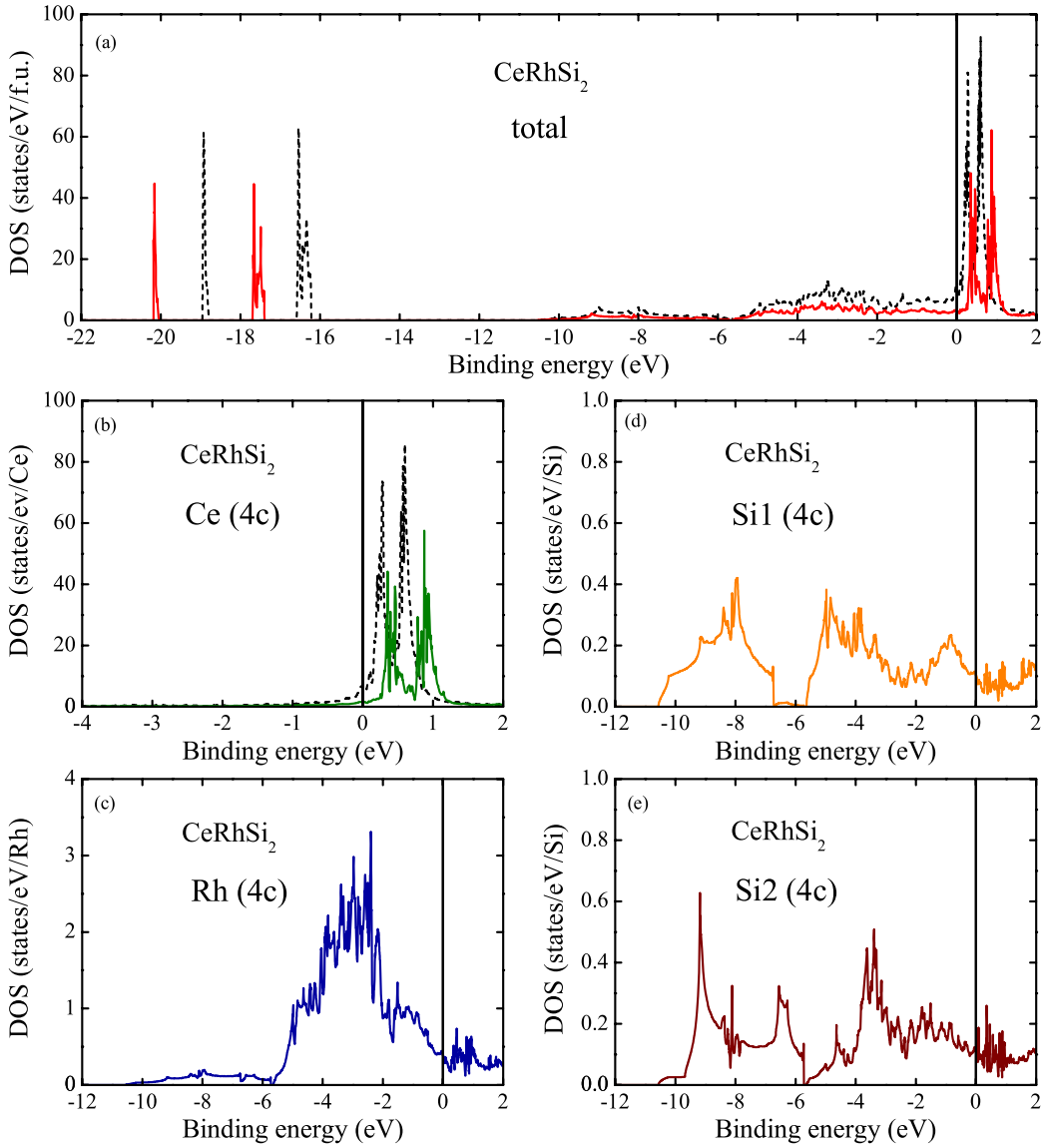

Figure 7. The total (per fu) and site projected (per atom) densities of electronic states (DOS) for $CeRhSi_2$ calculated within the LDA + U scheme (for comparison the total DOS and the Ce-atom DOS calculated using the LDA approach are presented by the broken line).

3.7. Electronic band structure

The band structure calculations performed using two distinct approaches, i.e. with FPLO and FP-LAPW, yielded very similar results and therefore only those obtained by using the WIEN2k code are discussed below. The latter method gives also an opportunity to go beyond LDA using the L(S)DA+U approach. The calculations were performed with and without spin polarization. The spin-polarized calculations were started with finite initial magnetic moments in order to promote magnetic solutions. However, the self-consistent results for magnetic solutions were nearly the same as those for nonmagnetic ones. In all the tests performed, the magnetic moments on cerium atoms were always below 10^{-7} μ_B/Ce atom for both $CeRhSi_2$ and $Ce_2Rh_3Si_5$.

The calculated densities of states (DOS) for the compounds $CeRhSi_2$ and $Ce_2Rh_3Si_5$ are presented in figures 7 and 8, respectively. In both cases the DOS plots can be divided into three parts below the Fermi level ($E_F = 0$). The first part located below -16 eV is composed of two peaks formed by the Ce($5p_{1/2}$) and Ce($5p_{3/2}$) electrons. It should be noticed that the LDA + U peaks are shifted towards higher binding energies. As will be discussed below, this shift improves the consistency between the calculated and measured x-ray photoelectron spectra, hence justifying the LDA+U approach. The second part, located between about -6 and -11 eV, is formed mainly by s electrons of the Rh and Si atoms. The third part, which is the main one of the valence bands, is located between the Fermi level and about -6 eV of the binding energy. The main contribution to these subbands is provided by d electrons located on the Rh atoms and Si(3p) electrons. A small contribution comes also from Ce(5d) electrons, but less than one electron per Ce atom. The Ce(4f) electrons form a narrow band with the center of gravity above the Fermi level. Most of the band is empty, and within the LDA scheme the number of occupied Ce(4f) states below E_f is equal to 0.92 for

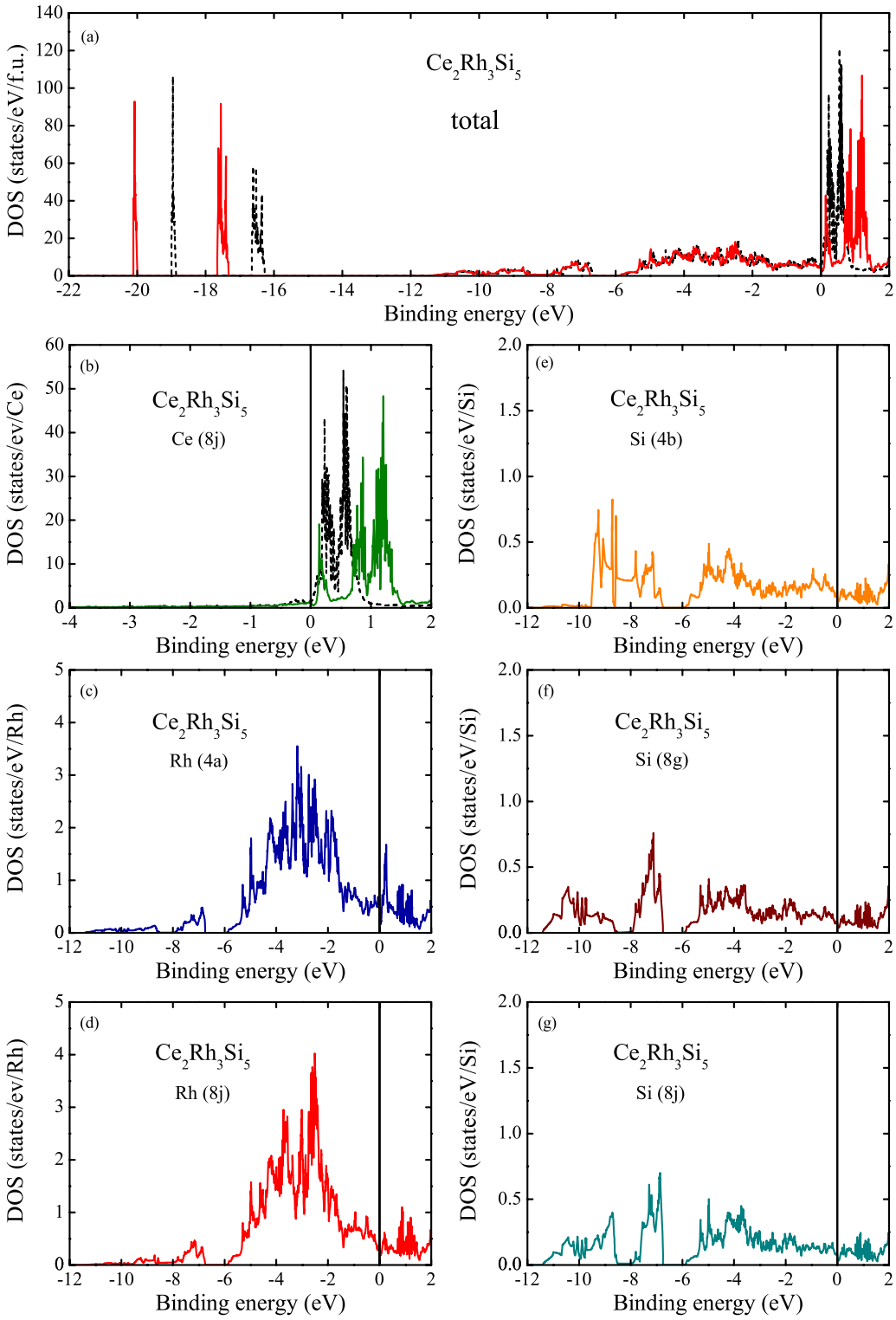

Figure 8. The total (per fu) and site projected (per atom) densities of electronic states (DOS) for $Ce_2R_3hSi_5$ calculated within the LDA + U scheme (for comparison the total DOS and the Ce-atom DOS calculated using the LDA approach are presented by the broken line).

both systems. The LDA + U calculations change the electronic structure in a way that the Ce(4f) band is slightly shifted above E_F and consequently the number of Ce(4f) electrons is reduced to 0.57 and 0.61 for $CeRhSi_2$ and $Ce_2Rh_3Si_5$, respectively. For the former compound, the occupation of electrons inside the atomic sphere of the Ce atom is given by the LDA approach as $6s^{1.98}5d^{0.64}4f^{0.92}$ and by the LDA + U calculations as $6s^{1.99}5d^{0.81}4f^{0.57}$. These results should be compared with the configurations $6s^25d^14f^1$ and $6s^25d^24f^0$ of Ce^{+3} and Ce^{+4} ions, respectively. Apparently, the calculated occupancies are intermediate between those characteristic for stable valence ions. Similarly, the results obtained for $Ce_2Rh_3Si_5$, which are

Table 3. DOS at E_F: total (per eV and fu) and site projected (per eV and atom) from orbitals giving the main contributions to the total value; calculated Sommerfeld coefficients γ_0 in mJ mol^{-1} K^{-2} and mass enhancement factors λ.

Compound	Type of calculation	Total	γ_0	λ	Ce(4f)	Rh1(4d)	Rh2(4d)
$CeRhSi_2$	LDA	4.92	11.60	6.4	2.87	0.32	—
	LDA + U	1.58	3.72	22.1	0.67	0.16	—
$Ce_2Rh_3Si_5$	LDA	4.73	11.15	3.2	1.19	0.55	0.19
	LDA + U	2.74	6.46	6.3	0.61	0.27	0.15

$6s^{1.98}5d^{0.67}4f^{0.92}$ and $6s^{1.99}5d^{0.82}4f^{0.61}$ for LDA and LDA + U calculations, respectively, also indicate distinct deviation from the stable valence configuration. This effect may be caused by additional charge transfer from/to rhodium and silicon atoms as well as by the charge accumulated in interstitial regions between atomic spheres.

The total DOS at E_F and the main contributions of particular atoms are summarized in table 3. The main contributions, about 50%, to the total DOS at E_F are provided by Ce(4f) electrons. Based on the DOS at E_F one can calculate the Sommerfeld coefficient γ_0, to be equal to about 11.6 and 11.2 mJ mol^{-1} K^{-2} for $CeRhSi_2$ and $Ce_2Rh_3Si_5$, respectively, obtained within the LDA approach and 3.7 and 6.5 mJ mol^{-1} K^{-2}, respectively, obtained with the LDA + U approach. Comparison of these values to the experimental ones (γ = 86 and 47 mJ mol^{-1} K^{-2}, for the two compounds, respectively) yields the mass enhancement factors $\lambda = (\gamma_{exp}/\gamma_0) - 1$, which are also collected in table 3.

Figure 9 presents the x-ray photoelectron spectra of $CeRhSi_2$ and $Ce_2Rh_3Si_5$, calculated from the DOS data using the cross sections reported in [28]. For comparison, the experimental XPS spectra are also shown. Apparently, the calculated results are quite consistent with the experimental ones. It should be noted that the LDA + U approach better describes the measured spectra for both systems, as judged from the distinct differences in the region of the Ce(5p) peaks.

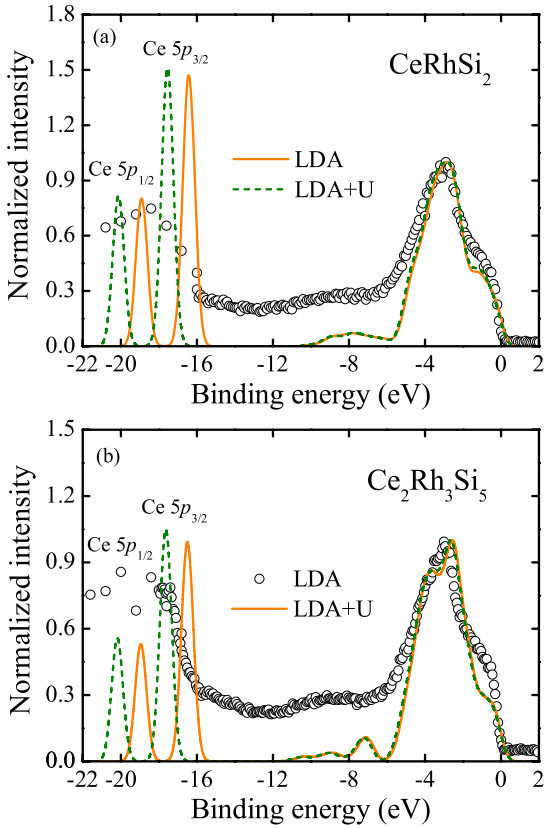

Figure 9. XPS valence band spectrum of (a) $CeRhSi_2$ and (b) $Ce_2Rh_3Si_5$, calculated within the LDA and LDA + U approaches and compared to the experimental one (represented by the symbols). Note the difference between the calculated spectra in the region of the 5p contribution.

4. Summary

The macroscopic and spectroscopic results obtained in this work for $CeRhSi_2$ and $Ce_2Rh_3Si_5$ unambiguously corroborate the intermediate valence character of both compounds. Mutually comparing the properties of these two phases it is worth noting that the effective valence of the Ce ion in $CeRhSi_2$ is closer to +3 than in the other silicide in the entire temperature range studied. In both compounds the electronic ground state of cerium is $4f^0$, yet the energy distance to the excited magnetic $4f^1$ state, E_{ex}, is smaller in $CeRhSi_2$ and hence the magnetic susceptibility of this compound is larger and more temperature-dependent than the susceptibility of the other one. Furthermore, stronger hybridization of the 4f electronic states with the conduction states in $Ce_2Rh_3Si_5$ is clearly reflected in larger values of the characteristic spin and charge fluctuation temperatures T_0 and T_{sf}. Similar conclusions as regards the valence states in the two compounds can be derived from the XAS and XPS results. The mean occupation of the 4f state is smaller in $Ce_2Rh_3Si_5$ and less temperature-dependent than in the other silicide, in line with the bulk magnetic data. The experimental XPS spectra can be fairly well reproduced by *ab initio* electronic band structure calculations, which yielded a nonmagnetic ground state in both compounds with significant mass enhancements due to strong electronic correlations.

Acknowledgments

The authors are grateful to Dr Marek Wołcyrz for collecting the x-ray powder diffraction data. This work was supported by the Ministry of Science and Higher Education within the research projects nos. N202 116 32/3270 and N202 1349 33. Part of the research was performed in the framework of the National Network 'Strongly correlated materials: preparation, fundamental research and applications'.

References

[1] Thalmeier P, Zwicknagl G, Stockert O, Sparn G and Steglich F 2005 *Frontiers in Superconducting Materials* ed A V Narlikar (Berlin: Springer) pp 109–82
[2] Kawarazaki S, Sato M, Miyako Y, Chigusa N, Watanabe K, Metoki N, Koike Y and Nishi M 2000 *Phys. Rev.* B **61** 4167
[3] Movshovich R, Graf T, Mandrus D, Thompson J D, Smith J L and Fisk Z 1996 *Phys. Rev.* B **53** 8241

[4] Araki S, Nakashima M, Settai R, Kobayashi T C and Onuki Y 2002 *J. Phys.: Condens. Matter* **14** L377
[5] Araki S, Settai R, Kobayashi T C, Harima H and Onuki Y 2001 *Phys. Rev.* B **64** 224417
[6] Muro Y, Eom D, Takeda N and Ishikawa M 1998 *J. Phys. Soc. Japan* **67** 3601
[7] Kimura N, Ito K, Saitoh K, Umeda Y, Aoki H and Terashima T 2005 *Phys. Rev. Lett.* **95** 247004
[8] Kimura N, Muro Y and Aoki H 2007 *J. Phys. Soc. Japan* **76** 051010
[9] Bauer E, Hilscher G, Michor H, Paul Ch, Scheidt E W, Gribanov A, Seropegin Yu, Noël H, Sigrist M and Rogl P 2004 *Phys. Rev. Lett.* **92** 027003
[10] Kimura N, Ito K, Aoki H, Uji S and Terashima T 2007 *Phys. Rev. Lett.* **98** 197001
[11] Kaczorowski D and Komatsubara T 2008 *Physica* B **403** 1362
Pikul A P and Kaczorowski D 2009 *Acta Phys. Polon.* A **115** 235
[12] Szlawska M, Kaczorowski D, Ślebarski A, Gulay L and Stepień-Damm J 2009 *Phys. Rev.* B **79** 134435
[13] Adroja D T and Rainford B D 1993 *J. Magn. Magn. Mater.* **119** 54
[14] Chevalier B, Rogl P, Hiebl K and Etourneau J 1993 *J. Solid State Chem.* **107** 327
[15] Godart C, Tomy C V, Gupta L C and Vijayaraghavan R 1988 *Solid State Commun.* **67** 677
[16] Ramakrishnan S, Patil N G, Chinchure A D and Marathe V R 2001 *Phys. Rev.* B **64** 064514
[17] Rodriguez-Carvajal J 1993 *Physica* B **192** 55
[18] Hohenberg P and Kohn W 1964 *Phys. Rev.* **136** B864
[19] Koepernik K and Eschrig H 1999 *Phys. Rev.* B **59** 1743
[20] Blaha P, Schwarz K, Madsen G K H, Kvasnicka D and Luitz J 2001 *WIEN2k, An Augmented Plane Wave + Local Orbitals Program for Calculating Crystal Properties* Karlheinz Schwarz, Techn. Universität Wien, Austria ISBN 3-9501031-1-2
[21] Perdew J P and Wang Y 1992 *Phys. Rev.* B **45** 13244
[22] MacDonald A H, Pickett W E and Koelling D D 1980 *J. Phys. C: Solid State Phys.* **13** 2675
[23] Perdew J P, Burke S and Ernzerhof M 1996 *Phys. Rev. Lett.* **77** 3865
[24] Wu Z and Cohen R 2006 *Phys. Rev.* B **73** 235116
Tran F, Laskowski R, Blaha P and Schwarz K 2007 *Phys. Rev.* B **75** 115131
[25] Anisimov V I, Solovyev I V, Korotin M A, Czyzyk M T and Sawatzky G A 1993 *Phys. Rev.* B **48** 16929
Liechtenstein A I, Anisimov V I and Zaanen J 1995 *Phys. Rev.* B **52** R5467
[26] Anisimov V I and Gunnarsson O 1991 *Phys. Rev.* B **43** 7570
[27] Blöchl P E, Jepsen O and Andersen O K 1994 *Phys. Rev.* B **49** 16223
[28] Yeh J J and Lindau I 1985 *Atom. Data Nucl. Data Tables* **32** 1
[29] Bodak O I and Gladyshevsky E I 1969 *Kristallografiya* **14** 990
Bodak O I and Gladyshevsky E I 1970 *Sov. Phys.—Crystallogr.* **14** 859 (Engl. Transl.)
[30] Lawrence J M, Riseborough P S and Parks R D 1981 *Rep. Prog. Phys.* **44** 1
[31] Béal-Monod M T and Lawrence J M 1980 *Phys. Rev.* B **21** 5400
[32] Sales B C and Wohlleben D K 1975 *Phys. Rev. Lett.* **35** 1240
[33] Röhler J 1987 *Handbook on the Physics and Chemistry of Rare Earths* vol 10, ed K A Gschneidner Jr, L Eyring and S Hüfner (Amsterdam: North-Holland) p 453
[34] Gopal E S R 1996 *Specific Heats at Low Temperatures* (New York: Plenum)
[35] Kittel C 2005 *Introduction to Solid State Physics* 8th edn (New Caledonia: Wiley)
[36] Wohlleben D and Wittershagen B 1985 *Adv. Phys.* **34** 403
[37] Moriya T 1985 *Spin Fluctuations in Itinerant Electron Magnetism* (Berlin: Springer)
[38] Gunnarsson O and Schönhammer K 1983 *Phys. Rev.* B **28** 4315
[39] Fuggle J C, Hillebrecht F U, Zolnierek Z, Lässer R, Freiburg Ch, Gunnarsson O and Schönhammer K 1983 *Phys. Rev.* B **27** 7330
[40] Anderson P W 1961 *Phys. Rev.* **124** 41
[41] Doniach S and Šunjić M 1970 *J. Phys. C: Solid State Phys.* **3** 286
[42] Tougaard S and Sigmund P 1982 *Phys. Rev.* B **25** 4452
[43] Ślebarski A, Zawada T, Spałek J and Jezierski A 2004 *Phys. Rev.* B **70** 235112
[44] Wuilloud E, Moser H R, Schneider W-D and Baer Y 1983 *Phys. Rev.* B **28** 7354
[45] Signorelli A J and Hayes R G 1973 *Phys. Rev.* B **8** 81
[46] Baer Y, Hauger R, Zürcher Ch, Campagna M and Wertheim G K 1978 *Phys. Rev.* B **18** 4433